Supporting Information

Hoopmann et al. 10.1073/pnas.1007037107

SI Materials and Methods

Reagents. Chemicals, buffers, and other reagents were purchased from Sigma–Aldrich or Merck unless otherwise specified. Tetraspeck beads (100 or 200 nm in diameter) and streptavidin-coated Qdots (525, 565, 605, and 655) were purchased from Invitrogen. The GFP-labeled Rab5 constructs were kind gifts from Mikael Simons (Max Planck Institute of Experimental Medicine, Gottingen, Germany); we have tested the construct activity previously in PC12 cell culture (1). The syntaxin 13-expressing system [GFP plasmid with soluble syntaxin 13 driven by an internal ribosomal entry site (IRES)] was organized as follows. Cells were transfected with the pIRES2-AcGFP1 Vector (Clontech), coding for the cytosolic domain of syntaxin 13 from rat (amino acids 1–250) and GFP. This vector ensures that the free (untagged) cytosolic fragment is expressed, avoiding tag-related problems; it also encodes for soluble GFP to ensure easy recognition of successful transfection. The expression of syntaxin 13 was confirmed by immunostaining in PC12 cells, with each GFP-positive cell also expressing cytosolic syntaxin 13. Similarly, we used a soluble syntaxin 13 construct lacking the SNARE domain (amino acids 1–186) cloned into the pIRES2-AcGFP1 Vector. Dynasore was purchased from ChemBridge Corporation and used at 80 μM. Methyl-β-cyclodextrin was purchased from Sigma–Aldrich.

Antibodies. In Fig. 2 *B–E*, we used the mouse monoclonal anti-synaptotagmin I 604.2 antibody (Synaptic Systems) coupled to Atto647N (Atto-tec) and rabbit polyclonal anti-GFP ab290 antibody (Abcam). Cy3-labeled goat anti-rabbit secondary antibodies were purchased from Dianova. For the positive colocalization control, we also used mouse monoclonal anti-synaptotagmin I 604.2 antibody coupled to Oyster550 (Synaptic Systems).

In Fig. 2 *F* and *G*, we used the mouse monoclonal anti-synaptotagmin I 604.2 antibody coupled to Atto647N.

In Fig. 3, we used the rabbit polyclonal anti-synaptophysin serum G96 (kind gift from Reinhard Jahn, Max Planck Institute for Biophysical Chemistry) (2). Cy3-conjugated goat anti-rabbit secondary antibodies were purchased from Dianova.

In Fig. 4 *A–E*, we used the mouse monoclonal anti-synaptotagmin I 604.2 antibody (Synaptic Systems), the mouse monoclonal anti-synaptotagmin I 604.2 antibody coupled to Atto647N, and the rabbit polyclonal anti-synaptophysin serum G96 (2). Goat anti-rabbit and anti-mouse secondary antibodies were purchased from Dianova and were coupled as described (3) with the dye Atto590 (Atto-tec).

In Fig. 4 *F–H*, we used the mouse monoclonal anti-synaptotagmin I 604.2 antibody coupled to Oyster550; mouse monoclonal anti-synaptobrevin 2 69.1 antibody (Synaptic Systems); mouse monoclonal anti-synaptotagmin I 41.1 antibody (Synaptic Systems); rabbit polyclonal anti-vglut1 shigeo2 serum (kind gift from Reinhard Jahn); rabbit polyclonal anti–GABA-transporter R22 serum (kind gift from Reinhard Jahn); mouse monoclonal anti-SNAP-25 71.1 antibody (Synaptic Systems); mouse monoclonal anti-syntaxin 1 HPC1 antibody (4); mouse monoclonal anti-clathrin heavy chain clone 23 antibody (BD Biosciences); rabbit polyclonal anti-dynamin 1,2,3 serum (Synaptic Systems); rabbit polyclonal anti-AP 180 serum (Synaptic Systems); rabbit polyclonal anti-endophilin serum (Synaptic Systems); rabbit polyclonal anti-synaptojanin 1 (C terminus) antibody affinity-purified from serum (Synaptic Systems); rabbit polyclonal anti-amphiphysin serum (Synaptic Systems); mouse monoclonal anti-uncoating ATPase 3C5 antibody (Synaptic Systems); mouse monoclonal anti–α-SNAP 77.1 antibody (Synaptic Systems); mouse monoclonal anti–*N*-ethylmaleimide-sensitive factor 83.11 antibody (Synaptic Systems); mouse monoclonal anti-Munc18-1 131.1 antibody (Synaptic Systems); mouse monoclonal anti–β-actin AC-15 antibody (Sigma–Aldrich); mouse monoclonal anti-vti1a 103.3 antibody (5); mouse monoclonal anti-syntaxin 6 clone 30 antibody (BD Biosciences); rabbit polyclonal anti-syntaxin 13 serum (5); mouse monoclonal anti-ADP Ribosylation Factor (Arf) 1D9 antibody (Abcam); rabbit polyclonal anti-AP1 complex subunit γ-1 serum (Affinity BioReagents); chicken polyclonal anti-AP3 β-2 serum (Abcam); mouse monoclonal anti-Rab4 clone 7 antibody (BD Biosciences); mouse monoclonal anti-Rab5 621.1 antibody (without fixation) (6); mouse monoclonal anti-PI3P Z-P003 antibody (Echelon Biosciences, Inc.); mouse monoclonal anti–HA-tag antibody (kind gift from Reinhard Jahn); mouse monoclonal anti-NMDA receptor 54.1 antibody (without fixation) (Synaptic Systems); rabbit polyclonal anti–voltage-gated Ca^{2+} channel antibody affinity purified from serum (Synaptic Systems); and rabbit polyclonal anti-synaptophysin serum G96 (2). Goat anti-mouse (Cy2- or Cy5-conjugated), goat anti-rabbit (Cy2- or Cy5-conjugated), and goat anti-chicken (Cy2-conjugated) antibodies were purchased from Dianova.

In Fig. S1, we used mouse monoclonal, Oyster550-coupled, anti-synaptotagmin I 604.2 antibody.

In Fig. S6, stainings were done exactly as in Fig. 3.

In Fig. S7 *A* and *B*, we used mouse monoclonal, Oyster550-coupled, anti-synaptotagmin I 604.2 antibody and mouse monoclonal anti-synaptotagmin I 604.2 antibody. Cy2-conjugated goat anti-mouse secondary antibodies were purchased from Dianova.

In Fig. S7 *C* and *D*, stainings were done exactly as in Fig. 4 *A–E*.

In Fig. S8 *A–C*, we used mouse monoclonal anti-SNAP-25 71.1 antibody, mouse monoclonal anti-syntaxin 1 HPC1 antibody (4), and rabbit polyclonal anti-synaptophysin serum G96 (2). Secondary goat anti-mouse antibodies were purchased from Dianova and coupled with the dye Atto647N, and goat anti-rabbit antibodies were purchased from Dianova and coupled with the dye Atto532 (Atto-tec).

In Fig. S8 *F–L*, stainings were done exactly as in Fig. 4 *F–H*.

In Fig. S8 *M* and *N*, we used mouse monoclonal anti-synaptogyrin 80.1 antibody (Synaptic Systems), rabbit polyclonal anti-Munc18 Struppi antibody (7), rabbit polyclonal anti-vamp8/endobrevin serum (8), mouse monoclonal anti-EEA1 clone 14 antibody (BD Biosciences), mouse monoclonal anti-vti1b clone 7 antibody (BD Biosciences), mouse monoclonal anti-syntaxin 7 109.1 antibody (kind gift from Reinhard Jahn), rabbit polyclonal anti-syntaxin 8 serum (9), mouse monoclonal anti–Rab-GDI 81.2 antibody (Synaptic Systems), mouse monoclonal anti-syntaxin 1 78.2 antibody (Synaptic Systems), mouse monoclonal anti-vti1a clone 45 antibody (BD Biosciences), rabbit polyclonal anti-syntaxin 6 serum (5), rabbit polyclonal anti-Rab4 serum (Abcam), mouse monoclonal anti-Rab5 621.3 antibody (without fixation) (I; Synaptic Systems), mouse monoclonal anti-Rab 5 clone 15 antibody (II; BD Biosciences), mouse monoclonal anti-synaptobrevin 2 69.1 antibody, and rabbit polyclonal anti-synaptophysin serum G96 (2). Goat anti-mouse (Cy2- or Cy5-conjugated) and goat anti-rabbit (Cy2- or Cy5-conjugated) antibodies were purchased from Dianova.

In Fig. S9, we used rabbit polyclonal anti–SNAP-25 serum (10), mouse monoclonal anti-syntaxin 1 78.2 antibody (Synaptic Systems), mouse monoclonal anti-synaptobrevin 2 antibody (Synaptic Systems), mouse monoclonal anti-synaptophysin 7.2 antibody (Synaptic Systems), and rabbit polyclonal anti-synaptophysin serum G96 (2). Goat anti-rabbit and anti-mouse secondary antibodies

were purchased from Dianova and were coupled as described (3) with the dye Atto590 or Atto647N.

In Movie S1, stainings were done exactly as in Fig. 2 *F* and *G*.

PHluorin Experiments. Superecliptic pHluorin was obtained with the agreement of the Sloan–Kettering Institute for Cancer Research (New York, NY). SynaptopHluorin was obtained from Leon Lagnado (Medical Research Council, Cambridge, United Kingdom). For the generation of the other SNARE-pHluorins (Fig. 1), a pHluorin entry vector was first constructed on the basis of the pEGFP-N1 vector (Clontech): pHluorin containing an N-terminal linker sequence (AGCGGCGGAAGCGGCGGGACCGGTGGA) was amplified by PCR from the SynaptopHluorin construct using the primers CGGGATCCAAGCGGCGGAAGCGGCGGGA and ATAGTTTAGCGGCCGCTCATGCCATGTGTATCCCAGC. The EGFP was replaced by this PCR fragment using BamHI and NotI. The SNAREs were amplified by PCR using the following primers: syntaxin 13, CCGCTCGAGcaccATGTCCTACGGTCCCTTAG and ACGTCACCGGTTCTTAGAAGCAACCCAGATAAC; syntaxin 6, ATCCGCTCGAGCACCATGTCCATGGAGGACCCCTTC and TATCGGGATCCCGCAGCACTAAGAAGAGGATGAGC; Vti1a, ATCCGCTCGAGCACCATGTCAGCCGACTTCGAAGG and TATCGGGATCCCGGTGTCCTCTGACAAAAAAAGTG; and syntaxin 1, ATCCGCTCGAGCACCATGAAGGACCGAACCCAGG and ATACGTCACCGGTTTCCAAAGATGCCCCCGATGG.

Syntaxin 1 and syntaxin 13 were cloned into the pHluorin entry vector via XhoI and AgeI/XmaI (SNARE PCR fragment cut with XhoI and AgeI, vector cut with XhoI and XmaI), and syntaxin 6 and Vti1a were cloned via XhoI and BamHI. For PCR reactions, the Phusion high-fidelity kit (New England Biolabs, Inc.) was used. The T4 ligase and all restriction enzymes were purchased from New England Biolabs, Inc. All constructs were sequenced by Eurofins MWG Operon.

All constructs were generated from rat (*Rattus norvegicus*) sequences.

Hippocampal cultures were prepared as described (11) and were transfected between 7 and 11 d in vitro (DIV) with the various pHluorin constructs using NeuroMag paramagnetic beads (Oz biosciences) according to the supplier's protocol. PHluorin imaging and analysis were performed largely as described (12). Cultures were stimulated using a platinum plate electrode (8-mm distance between the plates); 100-mA shocks were delivered using an A385 stimulus isolator and an A310 Accupulser stimulator (World Precision Instruments) at 20 Hz. Imaging was performed at 3.3 frames per second using an Olympus IX71 microscope equipped with a 0.75 N.A., 40× objective (Olympus); an F-View II CCD camera (1,376 × 1,032 pixels, pixel size of 6.45 × 6.45 μm; Olympus) using 2 × 2 pixel binning, and a GFP filter (480/40 HQ excitation filter, 505 long pass Q beamsplitter, and 527/30 HQ emission filter from the company AHF, Tübingen, Germany).

Photooxidation and EM. Hippocampal cultures (9–13 DIV, plated on Thermanox coverslips; Plano) were stimulated using the same stimulator as above, at 20 Hz for 2 s. FM dye was applied to the cultures for 10 s, followed by stimulation. The cultures were allowed to rest for various intervals (4, 10, and 30 s) before fixation by plunging in ice-cold glutaraldehyde [2.5% (wt/vol) in PBS]. The diaminobenzidine incubation and photoconversion were performed essentially as described (13) (Fig. S2), illuminating with a Zeiss Axioskop 2 microscope, equipped with an Olympus 20×, 0.5 N.A. objective. EM processing was performed as described (13). No poststaining of the sections was performed so as to allow for unambiguous identification of the labeled vesicles (Fig. S2*B*). Images were acquired using a Zeiss EM 902A electron microscope equipped with a 1024 × 1024 CCD detector (Proscan CCD HSS 512/1024; Proscan Electronic Systems). The vesicle diameters were determined by manually drawing line scans on the images using a routine written in Matlab (The Mathworks, Inc.).

Qdot Imaging. Hippocampal cultures were incubated with 5 μg/mL synaptotagmin luminal (intravesicular) domain antibodies (biotin-coupled) for 7 min on ice. After a brief wash, the antibodies were detected using streptavidin-coated Qdots, with a mixture of Qdot 525, Qdot 565, Qdot 605, and Qdot 655, each at a concentration of 10 nM (Fig. S2). The Qdots were then washed off, and the preparations were brought to room temperature; stimulated as above (20 Hz for 2 s); and fixed by plunging in ice-cold 4% (weight/vol) paraformaldehyde at 4, 10, or 30 s after stimulation. The preparations were quenched with 100 mM NH_4Cl and finally mounted in Mowiol (Calbiochem). They were imaged using a TCS (true confocal scanner) STED SP5 fluorescence microscope from Leica Microsystems GmbH, with a 1.4 N.A., 100× objective (Leica Microsystems GmbH). Excitation was performed at 488 nm with an argon laser line, and emission at the appropriate 20-nm interval (set via acousto-optical tunable filter) was detected using photomultipliers. The images were analyzed by finding the center of mass for each Qdot and then calculating the distance between each Qdot and its closest neighbor, irrespective of color (14). We used four different Qdot colors because this permits the high-precision positioning of four different types of vesicles simultaneously. Two identically labeled objects closer to each other than the diffraction of light cannot be separated. In contrast, objects from two different color channels can be positioned with a precision limited only by the signal-to-noise ratio and not by diffraction (discussed in 14).

Rab5-GFP Expression. Hippocampal cultures were prepared as described (11) and were transfected between 7 and 13 DIV with the GFP-Rab5 constructs using NeuroMag paramagnetic beads according to the supplier's protocol; alternatively, we used lipofectamine transfection (Lipofectamine 2000; Invitrogen) or CaPO4 transfection (15) (Fig. 2). Different transfection protocols were used to check whether any induce method-specific errors; because we could detect no substantial differences in the density of GFP-positive organelles or the general neuronal morphology, all results were pooled. After transfection (2–3 d), the preparations were incubated at 37 °C for 5 min in the presence of antibodies against the luminal (exposed) domain of synaptotagmin I (604.2) before fixation, permeabilization, secondary antibody incubation (goat anti-mouse coupled to Atto647N), and imaging; alternatively, we have used a directly labeled Atto647N-coupled 604.2 antibody. Stimulation experiments (Fig. 2*E*) were performed as above, except for the labeling step: Synaptotagmin epitopes were labeled on ice for 5 min (to prevent endocytosis), followed by returning to room temperature and stimulation using an RRP-releasing protocol (20 Hz/2 s) or a recycling pool-releasing protocol (20 Hz/30 s). The samples were fixed and processed after a 10-s break (as in Fig. S2).

Thin-Section Imaging. Sample processing was performed exactly as previously described (16). Imaging was performed using a TCS STED fluorescence microscope from Leica Microsystems GmbH, with a 1.4 N.A., 100× objective (Leica Microsystems GmbH) (Fig. 2 *B*–*E*). For STED imaging, excitation was performed with a 635-nm diode laser and depletion was achieved with a Spectra-Physics MaiTai tunable laser at 750 nm (Newport Spectra-Physics). Signal was detected with an avalanche photodiode. The system resolution limit is ~70–80 nm, measured by analysis of crimson-fluorescent beads (20-nm diameter; Invitrogen). GFP signal was observed by immunostaining the GFP moiety using the rabbit polyclonal ab290 antibody, detected via Cy3-labeled secondary antibodies. Imaging was performed in confocal mode using a HeNe laser (543 nm) for excitation and a photomultiplier tube for detection. Data analysis was performed using custom-written routines in Matlab as follows. Rectangular regions of interest (ROIs) were selected in areas

containing endosomes (identified in the GFP channel), and the area occupied by the (green) endosomes was determined by automatic thresholding (applying a threshold 1.5-fold higher than the mean of the ROI, which was empirically determined to function well for our ROIs); a similar threshold was applied to the red (synaptotagmin) image; and the amount of overlap was determined as the area of endosomes covered by vesicle staining (relative number of pixels). The values are expressed as a percentage of the control overlap. This was obtained by double-staining with two anti-synaptotagmin antibodies (604.2 coupled to Atto647N and 604.2 coupled to Oyster550) before fixation and thin-section processing, as described (16). The imaging was performed exactly as above; the overlap between the STED (Atto647N) synaptotagmin signal and the confocal (Oyster550) synaptotagmin signal was $27.55 \pm 2\%$ (mean ± SEM from three independent experiments) of the surface occupied by the confocal signal. Because the lower resolution of the Oyster550 imaging (single-spot FWHM ~267 nm) renders the Oyster550 spots substantially larger than the Atto647N spots, this result is to be expected.

For Fig. S8 *A* and *B*, sample processing was performed exactly as previously described (16). Imaging was performed with a TCS STED fluorescence microscope from Leica Microsystems GmbH as described above. Data analysis was performed as follows: ROIs (505-nm diameter circular regions) were selected in the centers of large synaptic vesicle (SV) clusters (identified in the synaptophysin channel), and the average fluorescence in the ROIs was calculated for both the synaptophysin and SNAP-25/syntaxin 1 channels. The fluorescence in SNAP-25/syntaxin 1, relative to that of synaptophysin, was then calculated and plotted as histograms.

Live STED Imaging. The imaging was performed using a live STED setup as described (3) (Fig. 2 *F* and *G* and Movie S1). To enable confocal resolution GFP imaging, we added a second pulsed laser diode (picoTA 490; Toptica) for excitation at 490 nm. The laser output was coupled into a polarization-maintaining single-mode fiber, and its collimated output was collinearly overlaid with the 637-nm excitation using a dichroic mirror. We added a second detection channel for the GFP emission by splitting the detection light after the confocal pinhole with a Semrock FF458 (which has a second edge at 609 nm) and guiding the lower wavelength portion through an HQ525-60m emission filter onto a second avalanche photodiode (SPCM-AQR13; Perkin–Elmer). Data analysis was performed using custom-written routines in Matlab as follows. Summed images were obtained by adding all frames of the movies. Rectangular ROIs were selected in the areas occupied by the endosomes, and the Pearson's correlation coefficients were calculated between the ROIs in the green (endosome, GFP) and red (vesicles, synaptotagmin) channels.

Syntaxin 13 Expression and Imaging. Neurons were grown as above. Soluble syntaxin 13 fragments were expressed from a GFP plasmid using an IRES (to avoid any tagging effects on the syntaxin fragment; see section on reagents) (Fig. 3 and Fig. S6). As a control, we expressed GFP alone to rule out the possibility that transfection/expression itself has any effect. At 1–2 d after transfection, the cells were either fixed and immunostained against synaptophysin (using Cy3-conjugated antibodies for secondary detection) to determine the total amount of vesicles or stimulated in presence of 10 μM FM 4-64FX (Invitrogen) for 2 s at 20 Hz (RRP-releasing protocol) or for 30 s at 20 Hz (protocol releasing all recycling vesicles). The preparations were allowed to recycle vesicles for 30 s before fixation. To check whether the RRP vesicles can be re-released, a second stimulation (30 s, 20 Hz) was performed after washing the preparations (for 10 min at room temperature), followed by fixation. For spontaneous pool labeling, the cells were incubated with 10 μM FM 4-64FX in the presence of 1 μM tetrodotoxin for 15 min. The preparations were then embedded in Mowiol and imaged with a TCS STED setup (see above). An Argon 488 laser line was used for GFP excitation, with a HeNe laser (543 nm) for FM 4-64FX and Cy3 excitation. The intensity of the vesicle labeling was determined by custom-written routines in Matlab; rectangular ROIs were selected in the GFP channel, the GFP signal was determined by automatic thresholding, and the average intensity of vesicle label in the corresponding area was measured.

Monte Carlo Modeling. Our model (Fig. 3) assumes the following: normal ($_n$) vesicles exist in the synapse; endocytosis occasionally retrieves improperly sorted vesicles (containing plasma membrane components), which we termed "dirty" for the sake of simplicity in the context of the model. Under normal circumstances, these vesicles would be sorted by the endosome. When the endosome activity is blocked, they accumulate and reduce RRP size because they have a lower ability to release than normal vesicles. To determine this unknown ability to release, we simulated an array of release abilities and obtained the RRP size in each of the conditions. The ability to release, which corresponds to a reduction of the RRP by ~60%, would explain the results obtained in living preparations (Fig. 3).

The response to a 20-AP train (at different frequencies) or, in other words, the RRP release was monitored first in the absence of any dirty vesicles, followed by a 30-s resting period. We then blocked endosomal sorting and allowed the accumulation of dirty vesicles during a prolonged activity period (1,000-AP train, 1 Hz); thus, the model reproduces a situation in which endosomal sorting is acutely inhibited. Because dirty vesicles will accumulate during this period, release on subsequent stimulation should be substantially reduced. To test the reduction in release after endosomal inhibition, a second 20-AP train was simulated. We recorded the amount of RRP release obtained on the second stimulus and expressed it as a ratio of the response on the first stimulus (color scale in Fig. 3*E*; "RRP % of control").

We expressed numbers used in the model as follows. We placed an RRP of 20 vesicles (n_n) (17) in the synapse. An identically sized pool of fused (readily retrievable) vesicles was in equilibrium with the RRP (nf_n) (18). No dirty vesicles (n_d) and no fused dirty vesicles (nf_d) were present at the start of the simulation. The probability of release for the normal vesicles (pr_n) was set to 0.3 (19), increasing under tetanic stimulation (5 Hz or above), so that it reached 1 at 20–30 Hz stimulation. The probability of release for the dirty vesicles (pr_d) was set to a variable fraction of the probability of release of the normal vesicles, with different fractions used for different models (pr_n/pr_d is plotted on the *y* axis in Fig. 3*E*). The probability of spontaneous release of the normal vesicles (ps_n) was set to once per minute (20); this value was adjusted to a higher level for the dirty vesicles (according to Fig. 3*C Right*). The probability that a normal vesicle is endocytosed (pe_n) was considered equal to the initial probability of release (0.3) so as to generate an accurate compensatory retrieval mechanism. The increased release probability during tetanic stimulation was compensated for by prolonged compensatory endocytosis [i.e., endocytosis continued at the same probability (0.3), which resulted in a temporary increase in the amount of vesicle membrane on the plasma membrane]. This increase was compensated for by allowing endocytosis to continue long after the stimulus, until the vesicle membrane added to the plasma membrane (by exocytosis) was endocytosed. Spontaneous release resulted in vesicles that were retrieved with the same probability of endocytosis for the sake of simplicity.

The probability of endocytosis for the dirty vesicles was set equal to that of the normal vesicles because, theoretically, they would both be targeted by the same release machinery (especially because both dirty and normal vesicles are retrieved simultaneously; Fig. 4 *F–H*). The probability that a dirty vesicle is retrieved was set to 0.4, corresponding to the proportion of newly

retrieved vesicles enriched in plasma membrane components (Fig. 4*H*; SNAP-25 and syntaxin 1).

Synaptic Vesicle Marker Surface Immunostaining. Hippocampal cultures were prepared as described (11) and were used between 8 and 34 DIV. To label the surface synaptic vesicle epitopes (Fig. 4 *A–E*), the cultures were incubated with fluorescently coupled antibodies against the luminal (exposed) domain of synaptotagmin I (604.2, coupled to the dye Atto647N) and a rabbit polyclonal serum which recognizes a luminal epitope of synaptophysin (G96) and were then fixed. Synaptophysin was visualized by immunostaining (without permeabilization) using goat anti-rabbit antibodies coupled with the dye Atto590.

To label specifically the recently exocytosed vesicles, we first incubated the preparations in Tyrode buffer [124 mM NaCl, 5 mM KCl, 2 mM $CaCl_2$, 1 mM $MgCl_2$, 30 mM glucose, 25 mM Hepes (pH 7.4)] in presence of unlabeled 604.2 antibodies (diluted 1:50 from ascites fluids; typically ~1–3 mg/mL antibody concentrations) for 10 min. Vesicle recycling was inhibited, because the incubation was either performed at 4 °C or in the absence of Mg^{2+} and Ca^{2+} at room temperature. After surface epitope blocking, we incubated the preparations with the fluorescently coupled anti-synaptotagmin antibody and anti-synaptophysin antibody (6 min, 4 °C, depolarizing with 15 mM KCl) (11). The preparations were fixed in 4% (weight/vol) paraformaldehyde for 10 min on ice, followed by 35 min at room temperature. Synaptophysin antibodies were stained by fluorescently coupled secondary antibodies before mounting the preparations in thiodiethanol (TDE). Alternatively, the positive colocalization control was performed without preblocking the surface; the incubations were performed without anti-synaptophysin antibodies, and secondary staining was performed with an Atto590-coupled anti-mouse secondary antibody after fixation (thus staining synaptotagmin with both Atto647N and Atto590).

The preparations were imaged using a dual-color STED microscope that combines two arrangements of excitation and STED laser beams. All beams were provided by a single supercontinuum laser source (SC-450 HP; Fianium), similar to a setup described previously (21). For excitation, the wavelengths were selected to be 570 ± 5 nm (Atto590) and 650 ± 5 nm (Atto647N); for the STED beams, wavelengths of 720 ± 10 nm (Atto590) and 755 ± 15 nm (Atto647N) were used. The fluorescence of the dyes is detected in the spectral ranges of 600–640 nm for Atto590 and 660–690 nm for Atto647N, respectively. Imaging was performed using a 1.4-N.A. oil objective lens (Plan Apochromat 100×/1.40–0.7 OIL; Leica Microsystems GmbH). Except for the elimination of crosstalk between the two detection channels by means of linear unmixing, the image data are raw data.

For analyzing spot diameters, we fitted line scans through the STED spots with Lorentzian curves (11) and determined the FWHM. The distance between intensity centers was analyzed exactly as described (14).

Single-Vesicle Immunostaining and Imaging. Synaptosomes were prepared and live-stained using a fluorescently labeled antibody against the luminal (exposed) domain of synaptotagmin I (604.2, coupled with the dye Oyster550) exactly as described (5) (Fig. 4 *F–H* and Fig. S8 *D–N*). The LS2 fraction enriched in synaptic vesicles (22) was removed and snap-frozen for long-term storage. We stimulated the synaptosomes by immersion in the KCl-containing solution for 5 min. This procedure is not in agreement with any of our other hippocampal culture stimulation paradigms, because synaptosomes are quite different in their release behavior. Only a small fraction of the vesicles recycled, as can be observed in the photoconversion example in Fig. S8*D*. Although it is debatable whether this vesicle fraction corresponds to the RRP, its size [about 2% of all vesicles were labeled in previous experiments (5)] places it on the order of magnitude of the RRP and much below the recycling or reserve pools.

To verify that this procedure is appropriate to label recycling vesicles in synaptosomes, we labeled synaptosomes with FM 1-43 as described (5) and processed the synaptosomes by photoconversion and EM (methods in Fig. S2; fixation was performed using 4% paraformaldehyde and 0.1% glutaraldehyde). For imaging single FM dye-labeled vesicles, we adsorbed the FM-labeled LS2 fractions onto glass coverslips and imaged them with a 100× 1.45-N.A. Total internal reflection fluorescence objective (Olympus) using a Zeiss Examiner.Z1 upright microscope and a QuantEM:512SC EM-CCD camera (Photometrics) with 512 × 512 pixels (pixel size: 16 × 16 μm).

For immunostaining experiments, the vesicles were adsorbed onto coverslips as described (5), fixed, and then incubated sequentially with antibodies against the protein of interest, followed by fluorescently labeled goat anti-mouse or anti-rabbit secondary antibody. Incubation with antibodies against a synaptic vesicle marker (typically, the anti-synaptophysin rabbit polyclonal G96 or the anti-synaptobrevin mouse monoclonal 69.1), followed by incubation with fluorescently labeled goat anti-rabbit or goat anti-mouse antibody, was then conducted. The preparations were then mounted in fluorescent mounting medium (Dako Denmark A/S) and imaged. We used the green (Cy2) channel for the protein of interest, the orange channel (Oyster550) for the anti-synaptotagmin antibody, and the deep red (Cy5) channel for the vesicle marker.

Imaging was performed using a Zeiss Axiovert 200M fluorescence microscope utilizing a 1.4-N.A., 100× objective (Zeiss) and a Princeton Instruments CCD camera with a 1317 × 1035 Kodak chip (pixel size: 6.8 × 6.8 μm). Green fluorescence was detected with the 480/40 HQ excitation filter, the 505 LP Q beamsplitter, and the 527/30 HQ emission filter. Orange fluorescence was detected using the 545/30 HQ excitation filter, the 570 LP Q beamsplitter, and the 610/75 HQ emission filter. Deep red (Cy5) fluorescence was detected using the 620/60 HQ excitation filter, the 660 LP Q beamsplitter, and the 700/75 HQ emission filter. The images were aligned by use of multicolor Tetraspeck beads (Invitrogen) as described (14). The beads were detected in blue fluorescence with the 350/50 D excitation filter, the 400 DCLP beamsplitter, and the 460/50 D emission filter (all filters were from Chroma). For comparison purposes, a number of datasets were taken using a second setup, an Olympus IX71 microscope equipped with a 1.4-N.A., 100× objective (Olympus); an F-View II CCD camera (1,376 × 1,032 pixels with a pixel size 6.45 × 6.45 μm; Olympus); and similar filters. The results were pooled, because no differences were found between the two setups beyond sample-to-sample variability.

Data analysis was performed using custom-written routines in Matlab. Briefly, the images were aligned as described (14); to increase the signal-to-noise ratio, images were filtered using an unsharp procedure (Matlab), followed by thresholding to identify the spots (vesicles; single pixels that surpassed the threshold were eliminated). Spots too large to represent single vesicles (but that were clumps of vesicles instead) were automatically eliminated from the analysis (size assessed on the basis of Gaussian fits performed on line scans through the spots). The threshold was automatically adjusted for each independent staining by using coverslips that had been treated similarly (i.e., immunostained) but without the addition of vesicles, which were thus essentially background controls. Line scans were performed automatically through the spots (selected in the synaptic vesicle marker channel, or in the luminal synaptotagmin antibody channel, to selectively identify the recently endocytosed vesicles), and the correlation between the signals in the different channels was calculated (Pearson's correlation coefficient). Correlation coefficients higher than 0.9 were considered to indicate colocalization of the spots. The analysis thus reported the number (or, more correctly, the fraction) of vesicles correlating with any of the proteins of interest investigated for both the general pool of vesicles and the recently endocytosed vesicles. Before plotting, the fractions were corrected for

random antibody colocalization (calculated in the coverslips immunostained without the addition of SVs).

Two-Color STED Imaging of Endosomes. PC12 endosomes were prepared by sucrose gradient centrifugation from PC12 postnuclear supernatants exactly as described (5). Synaptosomal organelles were prepared as above. They were centrifuged onto poly-L-lysine–coated coverslips, treated with methyl-β-cyclodextrin (60 mg/mL for 30 min), fixed, and immunostained exactly as described (23). After embedding in Mowiol, the endosomes were imaged as described above in the section on synaptic vesicle marker surface immunostaining and imaging (Fig. S9). For data analysis, the Pearson's correlation coefficient was determined for the green/red (Atto590/Atto647N) staining of individual endosomes.

PC12 Endosomal Trafficking. PC12 cells were cultured as described (24). All endocytotic probes and methods were used exactly as described (24) (Figs. S3 and S5). Data analysis was also performed as described (24).

Statistics. All data are presented as the mean ± SEM unless otherwise stated. To compare means (bar graphs), *t* tests were used; distributions were compared using Kolmogorov–Smirnov tests. When averages are presented, we avoided the use of single synaptic boutons in the statistics (e.g., in the fluorescent imaging of pHluorins or FM dye imaging); the statistics are shown as averages of independent experiments. This avoids the overrepresentation of experiments in which numerous boutons were analyzed.

1. Bethani I, et al. (2007) The specificity of SNARE pairing in biological membranes is mediated by both proof-reading and spatial segregation. *EMBO J* 26:3981–3992.
2. Jahn R, Schiebler W, Ouimet C, Greengard P (1985) A 38,000-dalton membrane protein (p38) present in synaptic vesicles. *Proc Natl Acad Sci USA* 82:4137–4141.
3. Westphal V, et al. (2008) Video-rate far-field optical nanoscopy dissects synaptic vesicle movement. *Science* 320:246–249.
4. Barnstable CJ, Hofstein R, Akagawa K (1985) A marker of early amacrine cell development in rat retina. *Brain Res* 352:286–290.
5. Rizzoli SO, et al. (2006) Evidence for early endosome-like fusion of recently endocytosed synaptic vesicles. *Traffic* 7:1163–1176.
6. Fischer von Mollard G, Stahl B, Li C, Südhof TC, Jahn R (1994) Rab proteins in regulated exocytosis. *Trends Biochem Sci* 19:164–168.
7. Zilly FE, Sørensen JB, Jahn R, Lang T (2006) Munc18-bound syntaxin readily forms SNARE complexes with synaptobrevin in native plasma membranes. *PLoS Biol* 4:e330.
8. Fasshauer D, Antonin W, Margittai M, Pabst S, Jahn R (1999) Mixed and non-cognate SNARE complexes. Characterization of assembly and biophysical properties. *J Biol Chem* 274:15440–15446.
9. Brandhorst D, et al. (2006) Homotypic fusion of early endosomes: SNAREs do not determine fusion specificity. *Proc Natl Acad Sci USA* 103:2701–2706.
10. Aguado F, et al. (1996) Expression of synaptosomal-associated protein SNAP-25 in endocrine anterior pituitary cells. *Eur J Cell Biol* 69:351–359.
11. Willig KI, Rizzoli SO, Westphal V, Jahn R, Hell SW (2006) STED microscopy reveals that synaptotagmin remains clustered after synaptic vesicle exocytosis. *Nature* 440: 935–939.
12. Mitchell SJ, Ryan TA (2004) Syntaxin-1A is excluded from recycling synaptic vesicles at nerve terminals. *J Neurosci* 24:4884–4888.
13. Rizzoli SO, Betz WJ (2004) The structural organization of the readily releasable pool of synaptic vesicles. *Science* 303:2037–2039.
14. Geumann U, Barysch SV, Hoopmann P, Jahn R, Rizzoli SO (2008) SNARE function is not involved in early endosome docking. *Mol Biol Cell* 19:5327–5337.
15. Xia Z, Dudek H, Miranti CK, Greenberg ME (1996) Calcium influx via the NMDA receptor induces immediate early gene transcription by a MAP kinase/ERK-dependent mechanism. *J Neurosci* 16:5425–5436.
16. Punge A, et al. (2008) 3D reconstruction of high-resolution STED microscope images. *Microsc Res Tech* 71:644–650.
17. Schikorski T, Stevens CF (2001) Morphological correlates of functionally defined synaptic vesicle populations. *Nat Neurosci* 4:391–395.
18. Wienisch M, Klingauf J (2006) Vesicular proteins exocytosed and subsequently retrieved by compensatory endocytosis are nonidentical. *Nat Neurosci* 9:1019–1027.
19. Gandhi SP, Stevens CF (2003) Three modes of synaptic vesicular recycling revealed by single-vesicle imaging. *Nature* 423:607–613.
20. Sara Y, Virmani T, Deák F, Liu X, Kavalali ET (2005) An isolated pool of vesicles recycles at rest and drives spontaneous neurotransmission. *Neuron* 45:563–573.
21. Wildanger D, Rittweger E, Kastrup L, Hell SW (2008) STED microscopy with a supercontinuum laser source. *Opt Express* 16:9614–9621.
22. Huttner WB, Schiebler W, Greengard P, De Camilli P (1983) Synapsin I (protein I), a nerve terminal-specific phosphoprotein. III. Its association with synaptic vesicles studied in a highly purified synaptic vesicle preparation. *J Cell Biol* 96:1374–1388.
23. Geumann U, Schafer C, Riedel D, Jahn R, Rizzoli SO (2010) Synaptic membrane proteins form stable microdomains in early endosomes. *Microsc Res Tech* 73:606–617.
24. Bethani I, et al. (2009) Endosomal fusion upon SNARE knockdown is maintained by residual SNARE activity and enhanced docking. *Traffic* 10:1543–1559.
25. Opazo F, et al. (2010) Limited intermixing of synaptic vesicle components upon vesicle recycling. *Traffic* 11:800–812.
26. Grabenbauer M, et al. (2005) Correlative microscopy and electron tomography of GFP through photooxidation. *Nat Methods* 2:857–862.

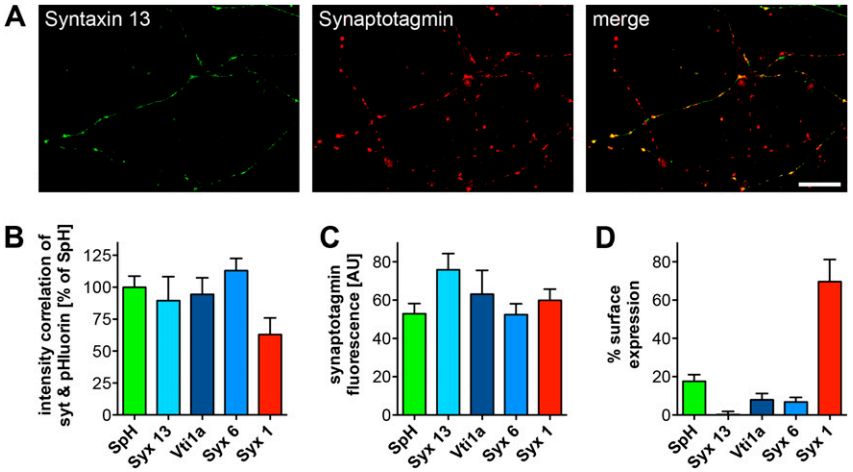

Fig. S1. The endosomal pHluorins do not inhibit vesicle recycling. (*A*) Syntaxin 13-pHluorin was expressed in hippocampal cultures. The cultures were allowed to recycle vesicles for 10 min in the presence of synaptotagmin antibodies coupled to the fluorescent dye Oyster550. The antibodies recognize the luminal domain of synaptotagmin and are taken up by endocytosis (in a much more specific synaptic uptake mechanism than, for example, FM dye uptake; shown in the cartoon in Fig. S2). Note the high correlation between syntaxin 13-pHluorin signal (green) and Oyster550 signal (red). (Scale bar: 25 μm.) (*B*) Quantification of the correlation between the pHluorin and synaptotagmin intensity. The correlation analysis was performed as follows. A threshold was applied to the pHluorin images, which eliminated background pixels. Thus, an ROI was obtained in which only pHluorin-positive pixels were found. We then calculated the Pearson's correlation coefficient between the intensities of the pixels within this ROI in the pHluorin and synaptotagmin channels. The values are expressed as a percentage of the synaptopHluorin correlation to synaptotagmin (thus using the well-studied synaptopHluorin as a control). The bars show the mean ± SEM for 7–23 independent experiments. (*C*) Quantification of the antibody uptake for the different pHluorins. The bars show the mean ± SEM for 8–20 independent experiments. No change was seen between synaptopHluorin and the pHluorin constructs. (*D*) Surface expression for the different pHluorins, indicated as a percentage of all pHluorin molecules. The bars show the mean ± SEM for 7–15 independent experiments; 10–60 synaptic boutons were analyzed in each experiment.

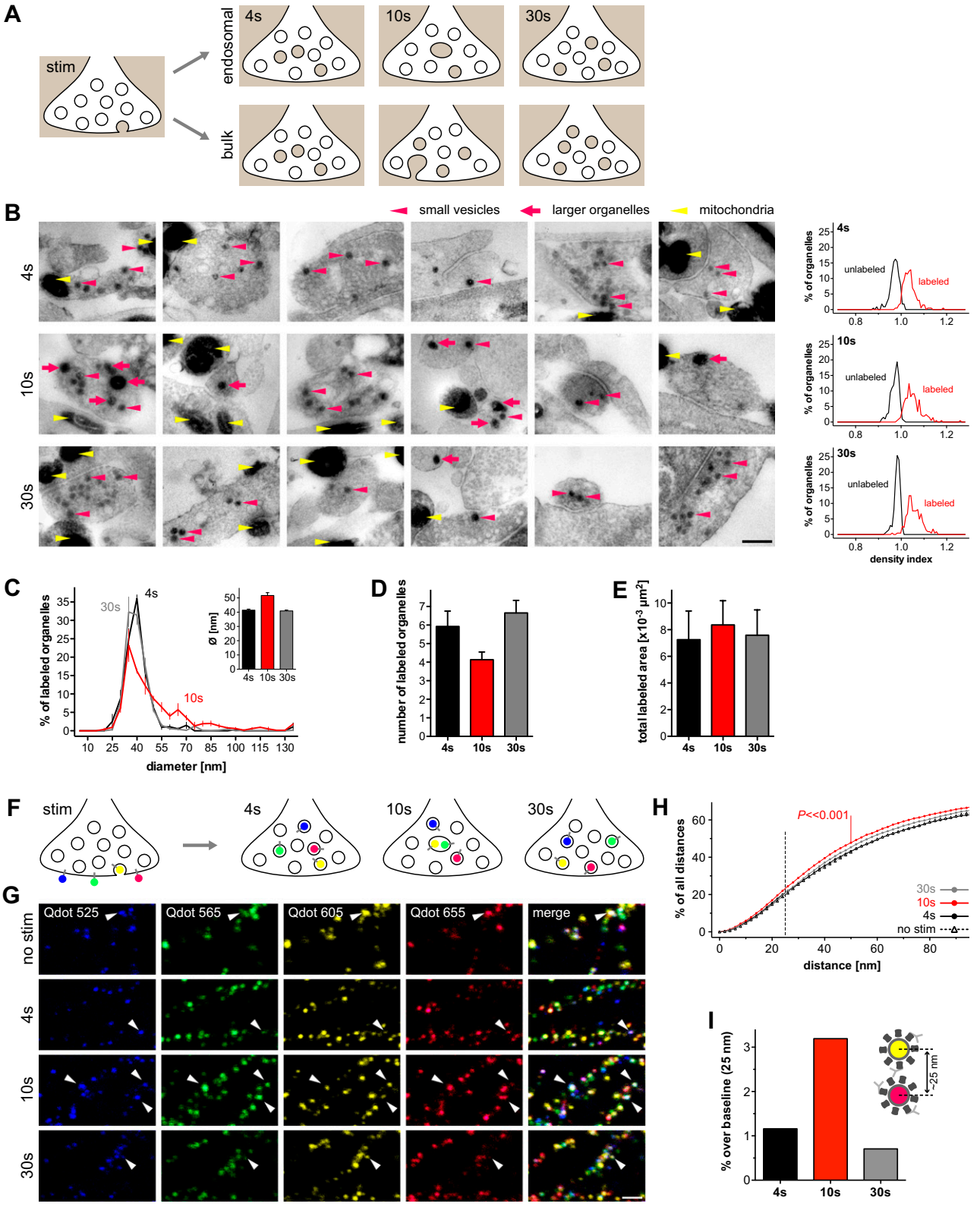

Fig. S2. Passage of RRP vesicles through endosomes. (*A*–*E*) Photooxidation analysis of FM dyes. (*A*) Hippocampal neurons are stimulated (20 Hz/2 s) in presence of FM 1-43, followed by fixation in ice-cold glutaraldehyde after a resting period of 4, 10, or 30 s. We observed a number of large labeled organelles (see below). Both endosomal and bulk endocytosis models can explain such organelles. In the endosomal model (*Upper*) the appearance of large organelles is accompanied by a reduction in the number of labeled objects; the amount of label stays constant. In the bulk endocytosis model (*Lower*) the appearance of large organelles is accompanied by increases in both the number of labeled objects and the amount of label. (*B*) Example micrographs of nerve terminals containing organelles labeled by di-amino-benzidine photooxidation of FM 1-43 (refs. 13 and 25). (Scale bar: 200 nm.) Note that mitochondria label in this procedure as well (yellow arrowheads), although this is independent of the presence of FM dyes (26). Red arrowheads/arrows point to examples of small and large vesicles, respectively; not all vesicles are indicated. The plots on the right side indicate the relative density distributions from vesicles identified as un-

Legend continued on following page

labeled (black) or labeled (red). The relative density is the ratio between the density of the vesicle lumen and the vesicle membrane (<1 unlabeled vesicles, >1 for labeled vesicles) (13). Note that unlabeled and labeled vesicles are easily distinguished, with the two distributions well differentiated. The graphs show histograms from at least 200 vesicles for each condition. (*C*) Labeled vesicle size (diameter). Large labeled vesicles (~50–100 nm) appear after 10 s, and disappear after 30 s of rest. The size distribution at 10 s after stimulation is significantly different from the others ($P < 0.01$, KS tests). *Inset* shows the average vesicle diameter (significantly larger in the 10-s condition, $P < 0.01$, *t* tests). (*D*) Number of labeled organelles per micrograph (significantly smaller in the 10-s condition; $P < 0.05$, *t* tests). (*E*) Total labeled area. The *t* tests were unable to demonstrate significant differences between the different conditions. The data in *C–E* were obtained from three independent experiments, with 140–195 electron micrographs analyzed. All graphs show means +/– SEM. (*F–I*) The Qdot endocytosis assay. (*F*) Exocytosed vesicles are labeled by a biotinylated antibody directed against the lumenal (intravesicular) domain of synaptotagmin, followed by addition of streptavidin-coated Qdots. Stimulation (20 Hz/2 s) results in Qdot endocytosis. If endosomal recycling takes place, Qdots tightly pressed against each other should appear after vesicular fusion to the endosome and should later separate through vesicle budding. (*G*) Typical images of nerve terminals labeled with four different Qdots, at different intervals after stimulation. (Scale bar: 1.5 μm.) Arrowheads point to example organelles where at least four Qdots colocalize. (*H*) The minimal distances between the differently colored Qdots were analyzed, and cumulative histograms were plotted for nerve terminals either before stimulation or at 4, 10, and 30 s after stimulation. The distribution at 10 s after stimulation is significantly different from all other three distributions ($P < 0.001$, *t* tests). The same test was unable to demonstrate significant differences between the nonstimulated preparations and those at 4 or 30 s after stimulation. The vertical dotted line indicates a distance between the Qdots of 25 nm. The histograms were obtained from ~8,000 to 14,000 Qdot distances, from three independent experiments. (*I*) Amount of Qdots within less than 25 nm from other Qdots (i.e., tightly apposed, *Inset*). The values were corrected for the positioning of Qdots before stimulation; closely apposed Qdots before stimulation are likely bound to single multi-biotinylated antibodies, and therefore are not biologically meaningful.

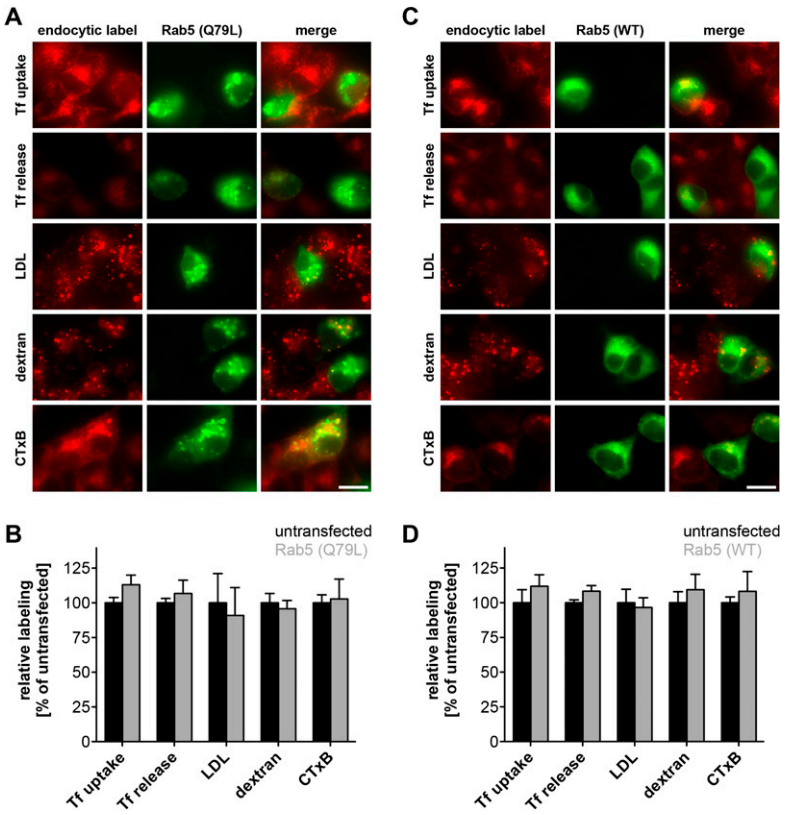

Fig. S3. Expression of GFP-tagged Rab5 variants (WT or Q79L) does not affect endosomal trafficking in PC12 cells. (*A*) Typical images of PC12 cell fields containing both cells expressing Rab5 Q79L-GFP (green) and control untransfected cells. Several endocytic labels were used (all shown in red). For transferrin (Tf) uptake, cells were incubated for 5 min at 37 °C with 50 μg/mL Tf-Alexa594; for Tf release, cells were labeled in the same fashion, were briefly washed (twice), and were incubated at 37 °C for an additional 10 min in the absence of Tf. For LDL uptake, cells were incubated for 5 min at 37 °C with 5 μg/mL LDL-DiI. For dextran uptake, cells were incubated for 5 min at 37 °C with 1 mg/mL dextran-Alexa594. For cholera toxin β-subunit (CTxB) uptake, cells were preincubated for 30 min on ice with 10 μg/mL CTxB-Alexa647. After briefly washing three times, the cells were incubated for another 40 min at 37 °C to allow the toxin to reach the Golgi. (Scale: 15 μm.) (*B*) Quantification of the endocytotic labeling. The red (endocytotic marker) fluorescence of PC12 cells expressing GFP-tagged dominant active Rab5 (Q79L) was normalized to the fluorescence of untransfected cells. The *t* tests were unable to demonstrate significant differences between the different conditions. (*C* and *D*) Same experiments were repeated using the WT variant of Rab5 coupled to GFP. Again, the *t* tests were unable to demonstrate significant differences between the different conditions. Quantification represents the means ± SEM of four experiments.

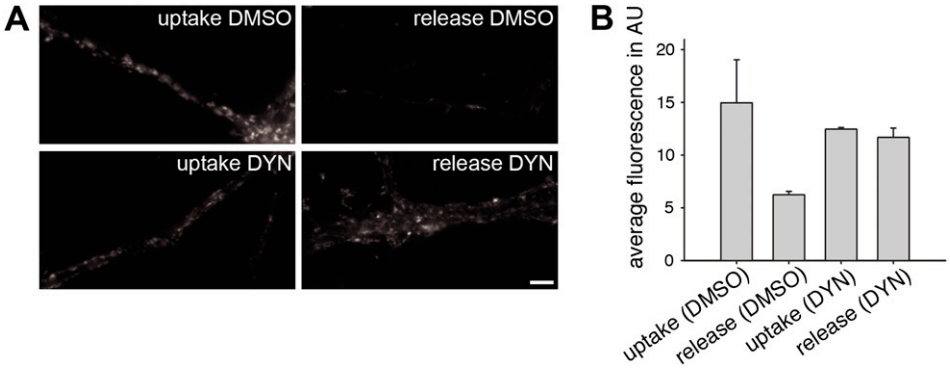

Fig. S4. Dynasore inhibits synaptic vesicle recycling. (*A*) FM uptake and release. Cultured hippocampal neurons were incubated for 10 min at 37 °C in presence of 80 μM Dynasore or in presence of a corresponding amount of solvent (DMSO). After incubation, they were briefly washed and were stimulated in presence of the styryl dye FM 2-10 (by application of 70 mM KCl for 5 min). After a brief dye wash-off, the preparations were either immediately imaged to obtain an image of the dye uptake (*Left*, labeled "uptake") or were subjected to a second round of KCl stimulation in absence of the dye, which causes dye release from the vesicles, before imaging (*Right*, labeled "release"). (Scale bar: 5 μm.) (*B*) Quantification of synaptic fluorescence. The fluorescence (above background) of the images was measured from two independent experiments with a self-written routine in Matlab. The bars show the mean ± range of values. Note that release of the dye is completely blocked by Dynasore, indicative of inhibited vesicle recycling.

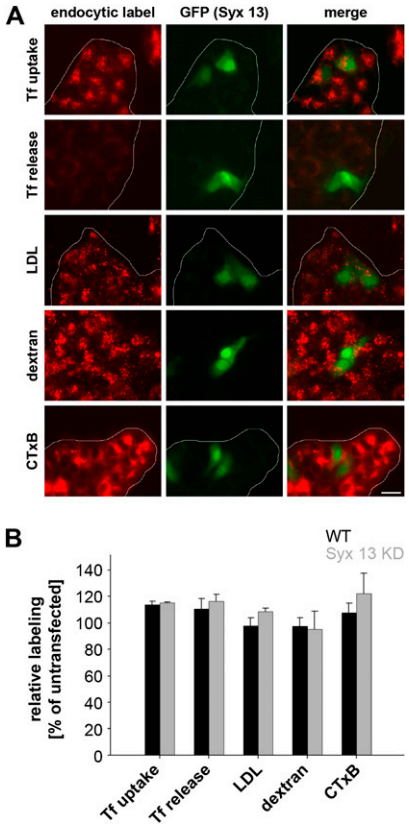

Fig. S5. Effects of expressing soluble syntaxin 13 on endosomal trafficking in PC12 cells. (*A*) WT and syntaxin 13 knockdown (Syx 13 KD) cells were transfected with a pIRES vector coding for the cytosolic domain of syntaxin 13. This vector ensures that the free (untagged) cytosolic fragment is expressed, avoiding tag-related problems; it also encodes for free GFP for easy recognition of successful transfection. The cells were allowed to internalize fluorescently labeled transferrin (Tf), LDL, dextran, or cholera toxin β-subunit (24). Images show syntaxin 13 knockdown cells; WT cells behaved similarly. We tested the knockdown cells because they only contain about 10% of the original syntaxin 13, and therefore should be especially sensitive to any damaging effects of expressing soluble syntaxin 13 fragments. (Scale bar: 10 μm.) (*B*) Amount of marker internalized (and, for Tf, also recycled) was quantified both in cells expressing syntaxin 13/GFP and in the neighboring untransfected (control) cells. The values obtained in the transfected cells were normalized to those in the control cells. Note that no reductions (perturbations) in endosomal function in the transfected cells could be demonstrated by use of *t* test. Quantification shows the mean ± range of values in two independent experiments.

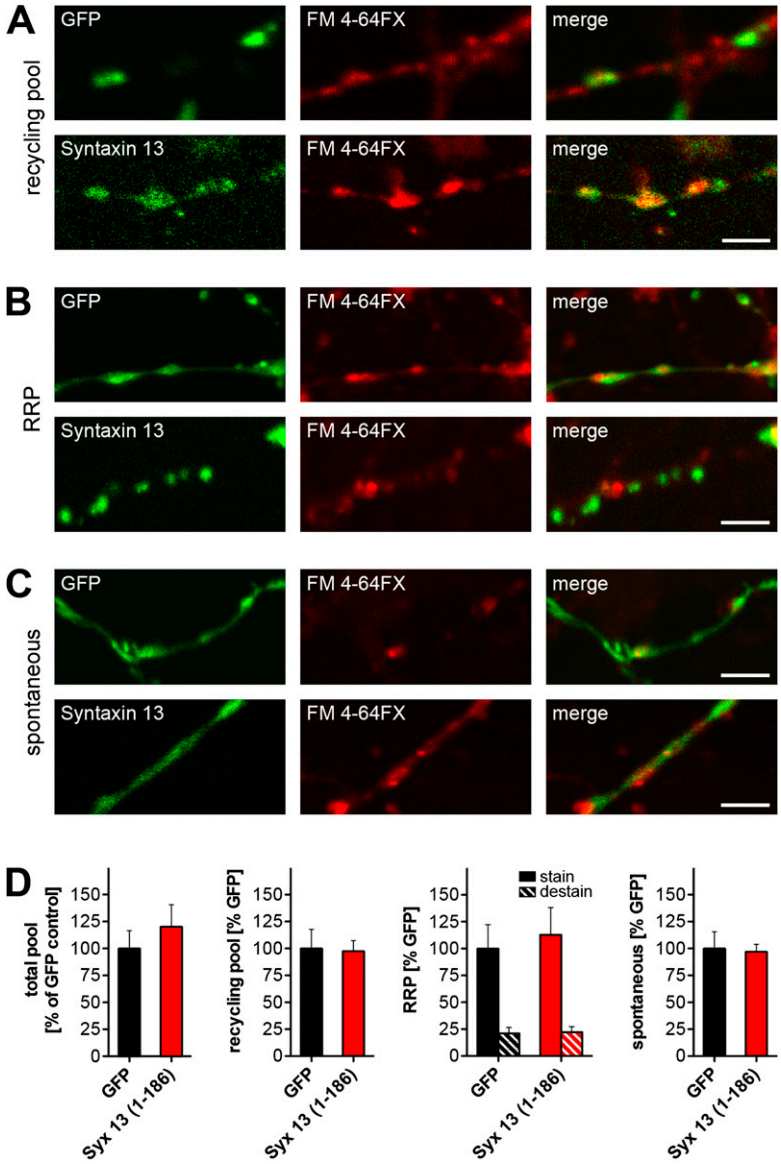

Fig. S6. FM dye uptake in preparations expressing soluble syntaxin 13 fragments. (*A–C*) Labeling examples for vesicle pools, as in Fig. 3. Note that the quantification of these experiments is presented in Fig. 3. Hippocampal cultures expressing either GFP alone (*Upper*) or GFP and the soluble syntaxin 13 fragment (*Lower*) were incubated with FM 4-64FX (10 μM) and were stimulated for 30 s at 20 Hz (recycling pool labeling protocol) (*A*), stimulated for 2 s at 20 Hz (RRP labeling protocol) (*B*), and incubated for 15 min in presence of 1 μM tetrodotoxin (spontaneous pool labeling protocol) (*C*). (Scale bar: 2.5 μm.) (*D*) Quantification of vesicle pools on expression of syntaxin 13 lacking the SNARE domain (amino acids 1–186). All pools are expressed as a percentage of the GFP-only control. (*Left*) Total pool was quantified from synaptophysin immunostaining. The recycling pool and the RRP were labeled with FM 4-64FX by stimulating at 20 Hz for 30 and 2 s, respectively. Note that the FM-loaded RRP vesicles could be re-released by a 20-Hz/30-s stimulus in both conditions ("destain," hashed bars). Spontaneously recycling vesicles were labeled by incubation with FM 4-64FX for 15 min in presence of 1 μM tetrodotoxin. Note that expression of syntaxin 13 fragments lacking the SNARE domain does not exhibit any vesicle pool-related effects. Data are presented as the mean ± SEM from two to four independent experiments.

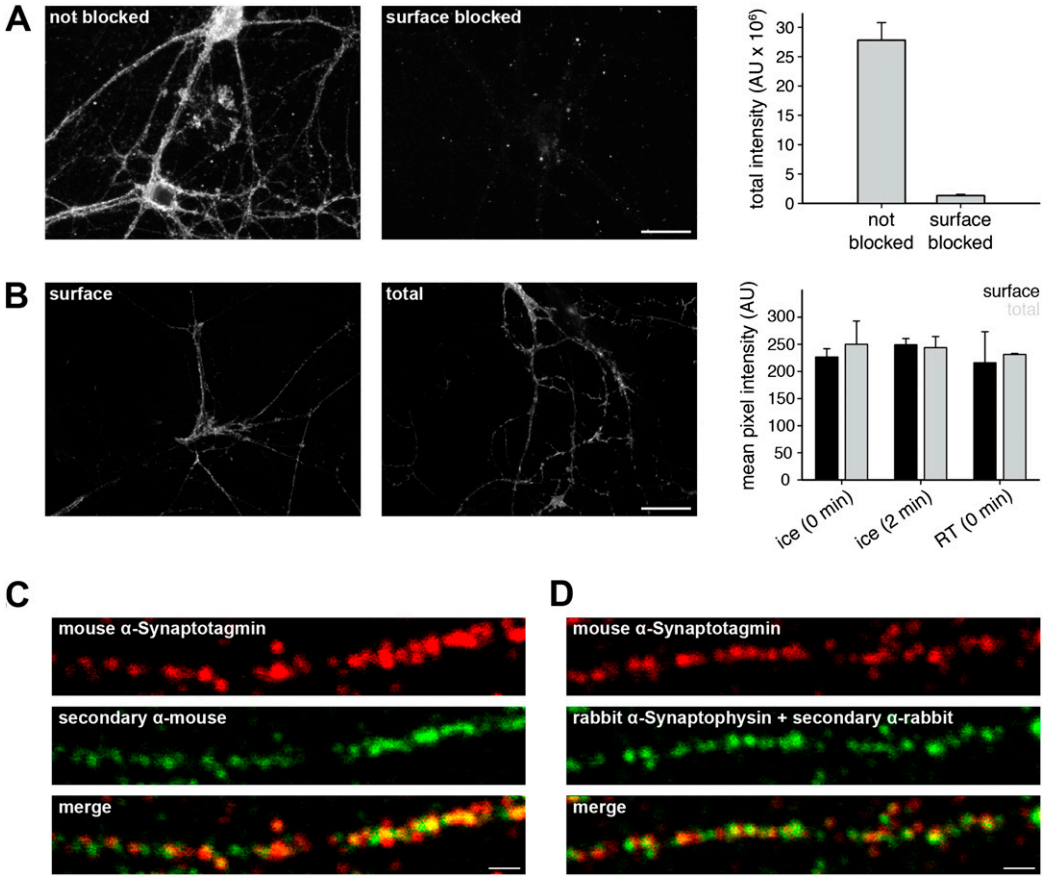

Fig. S7. Study of recently exocytosed vesicle markers. (*A* and *B*) Blocking surface synaptotagmin epitopes and inhibition of endocytosis allow the specific investigation of recently exocytosed vesicles. (*A*) Blocking preexisting synaptotagmin surface epitopes before stimulating exocytosis. Hippocampal neurons were stained with fluorescently coupled antibodies against the luminal domain of synaptotagmin either without (*Left*) or with (*Center*) a preceding treatment with unlabeled anti-synaptotagmin antibodies. Surface blocking drastically reduced the total intensity (graph). (Scale bar: 25 μm.) (*B*) Endocytosis block to avoid investigation of reinternalized vesicles. To investigate surface staining of synaptotagmin, the endocytosis of the recently fused vesicles needed to be avoided (because not avoiding endocytosis would have resulted in the analysis of endocytosed synaptotagmin-labeled synaptic vesicles instead of plasma membrane-exposed material). Therefore, the labeling was performed either at 4 °C or in the absence of Mg^{2+} and Ca^{2+} at room temperature (RT) to allow for exocytosis (compare with synaptotagmin signal in Fig. 4) but not endocytosis. To test the endocytosis block, we labeled hippocampal neurons with primary antibodies against the luminal domain of synaptotagmin, fixed them (immediately after a brief ice-cold wash or with an additional incubation on ice for 2 min), and stained them with secondary fluorescent antibodies either without (*Left*, surface) or with (*Center*, total) permeabilization. The fluorescence intensity quantification reveals that permeabilized and nonpermeabilized samples appear to be similar, underscoring the fact that the chosen labeling conditions effectively result in all synaptotagmin antibodies persisting at the surface (i.e., block of endocytosis) even after a short incubation of the preparations after labeling. (Scale bar: 25 μm.) (C and *D*) Limited resolution in confocal images only allows for a crude interpretation of synaptotagmin/synaptophysin colocalization. The same areas as in Fig. 4 *A* and *B* are imaged. (*C*) Colocalization control experiment. Neurons are incubated for 6 min with fluorescently-coupled mouse monoclonal antibodies that recognize the luminal domain of synaptotagmin (red). After fixation, the samples are immunostained with secondary anti-mouse antibodies (green). (Scale bar: 1 μm.) (*D*) Synaptotagmin/synaptophysin colocalization. Neurons are incubated for 6 min with fluorescently-coupled mouse antibodies that recognize the luminal domain of synaptotagmin (red) and rabbit antibodies that recognize the luminal domain of synaptophysin. After fixation, the samples are immunostained with secondary anti-rabbit antibodies (green) to visualize the synaptophysin staining. (Scale bar: 1 μm.)

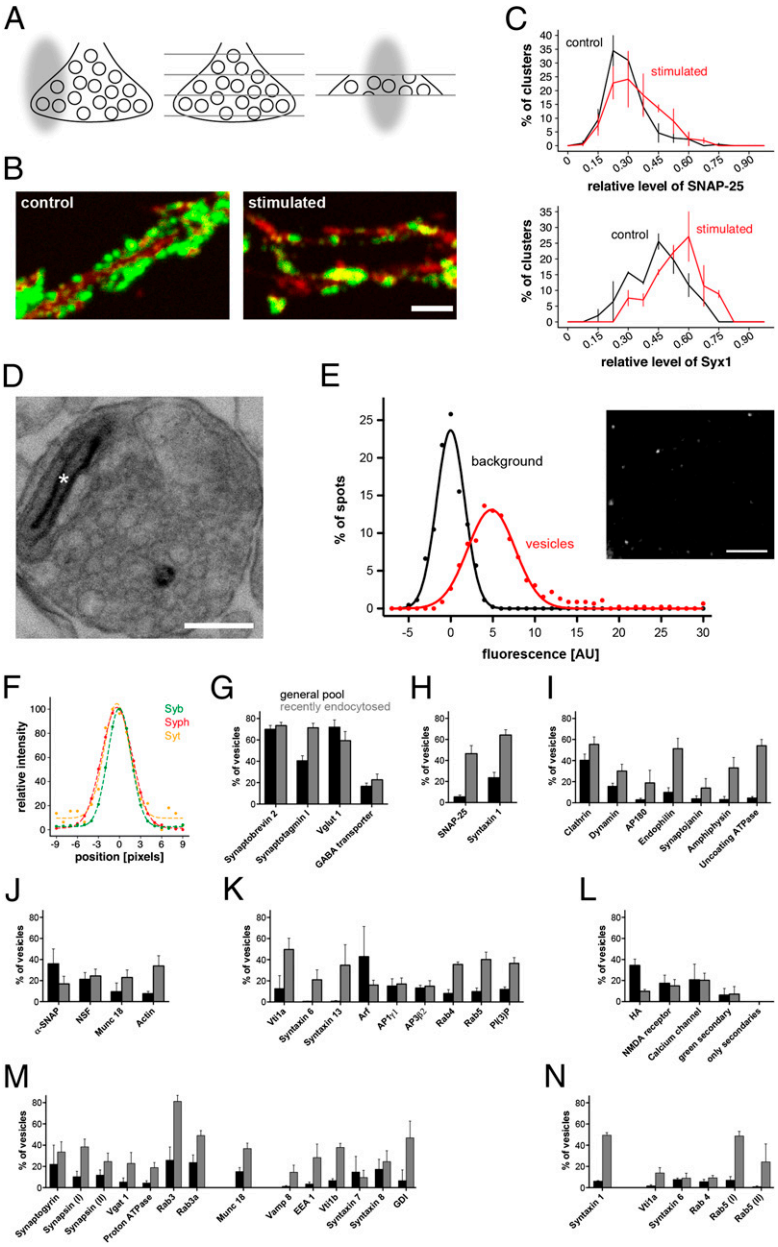

Fig. S8. Study of the composition of recently endocytosed vesicles. (*A–C*) Stimulation increases the amount of syntaxin 1/SNAP-25 in vesicle clusters. To test whether plasma membrane components would be more abundant in vesicles after recycling, we stimulated neuronal cultures by KCl depolarization (as for the synaptosomes in Fig. 4) and then immunostained them for the synaptic vesicle marker synaptophysin and for the membrane-resident proteins SNAP-25 or syntaxin 1. Because the poor axial (Z) resolution of conventional microscopy (~600 nm) does not allow the distinction between syntaxin 1/SNAP-25 present either on the membrane or within the vesicle clusters, we embedded the preparations in plastic material and cut them into ultrathin sections. (*A*) Schematic representation of the experimental procedure. Poor axial (Z) resolution in light microscopy does not allow distinguishing the plasma membrane from the vesicle clusters within the bouton interior. In contrast, thin sectioning (~80 nm) allows for selective investigation of SV clusters. (*B*) Control (*Left*) or stimulated (*Right*; 70 mM KCl) hippocampal cultures were immunostained for synaptophysin (green) and for SNAP-25 (red), followed by sectioning. Note the increase of signal colocalization after stimulation (the increase of SNAP-25 signal in large synaptic vesicle clusters). (Scale bar: 2 μm.) (*C*) Quantification of the relative SNAP-25 (*Upper*) or syntaxin 1 (Syx1; *Lower*) intensity within the vesicle clusters. Graphs show the mean ± SEM for SNAP-25 (three independent experiments) and the mean ± range of values for syntaxin 1 (two independent experiments). The distributions are significantly different for both syntaxin 1 and SNAP-25 ($P < 0.01$, Kolmogorov–Smirnov test). We conclude that the plasma membrane proteins do enrich in synaptic vesicle clusters after stimulation, which, however, is in agreement with both the bulk endocytosis and endosomal recycling models (as in Fig. 1*A*). (*D–E*) Endocytosis of small vesicles in synaptosomes. (*D*) Synaptosomal preparations were labeled with FM 1-43 (with a 50-mM KCl stimulation), and the electron-dense diaminobenzidine precipitate was generated by photooxidation (as in Fig. S2). The micrograph shows one labeled vesicle. Note that the large dark structure marked by an asterisk in the top left corner is a mitochondrion (labeled by diaminobenzidine independent of the FM 1-43 presence (26). (Scale bar: 200 nm.) (*E*) Intensity histograms of FM-labeled vesicles adsorbed onto glass coverslips. Background intensity (black) follows an almost perfect Gaussian fit with a peak around zero intensity. The intensities of the vesicles (red) are also normally distributed. Data points show the actual distribution, and line plots are Gaussian fits. (*Inset*) Example image of labeled vesicles (the image was smoothed for display, because the signal-to-noise ratio is fairly low). (Scale bar: 5 μm.) We conclude that the vesicle labeling is normally distributed, indicating a relatively homogeneous pool of small (as in *D*) vesicles, with few larger organelles. Larger organelles would necessarily be brighter, because FM fluorescence is directly proportional to the amount of membrane labeled. (*F–N*) Immunostaining of isolated synaptic vesicles to study the

Legend continued on following page

composition of general pool vesicles vs. recently endocytosed vesicles. (*F*) Example of line scans through a spot (vesicle) colocalizing in all three channels. Data points show raw data (normalized to 100 AU), and dashed lines are Gaussian fits. Colocalization was assessed based on the correlation coefficient between the different signals (*SI Materials and Methods*). (*G*–*N*) Detection of various proteins of interest in general pool vesicles (black) vs. recently endocytosed vesicles (gray). (*G*) Synaptic vesicle proteins. These proteins are generally present on the same amount of general pool vesicles as recently endocytosed vesicles. Note that the increase seen for synaptotagmin I is probably attributable to the fact that the recently endocytosed vesicles are identified by the presence of synaptotagmin I epitopes (luminal), whereas the general pool vesicles could also be lacking synaptotagmin I and contain other synaptotagmin isoforms. (*H*) Plasma membrane proteins. SNAP-25 and syntaxin 1 are present on more recently endocytosed vesicles than general pool vesicles. (*I*) Clathrin-mediated endocytosis machinery. Some components of the classic endocytosis machinery can be found on more recently endocytosed vesicles compared with general pool vesicles. (*J*) Soluble proteins. These proteins are generally associated with relatively low amounts of vesicles. (*K*) Endosomal components. Several endosomal components can be found on more recently endocytosed vesicles. (*L*) Controls. Staining for nonsynaptic protein (HA) and for pre- and postsynaptic ion channels (calcium channel, NMDA receptor) shows that the assay does not detect an increase in the amount of recently endocytosed vesicles containing various proteins "by default." We cannot exclude, however, the possibility that values in the detection range of ~10–20% may be attributable to unspecific staining. Other controls are "green secondary" (immunostaining for synaptophysin as the synaptic vesicle marker and immunostaining with only anti-mouse secondary antibodies as proteins of interest) and "only secondaries" (immunostaining with only anti-rabbit secondary antibodies as the synaptic vesicle marker and immunostaining with only anti-mouse secondary antibodies as proteins of interest). (*M*) Several additional protein targets not included in Fig. 4 because of space constraints. (*N*) Retesting of several protein targets from Fig. 4 using different antibodies. Note that the results generally correlate, although several antibodies detect their targets on very low numbers of vesicles.

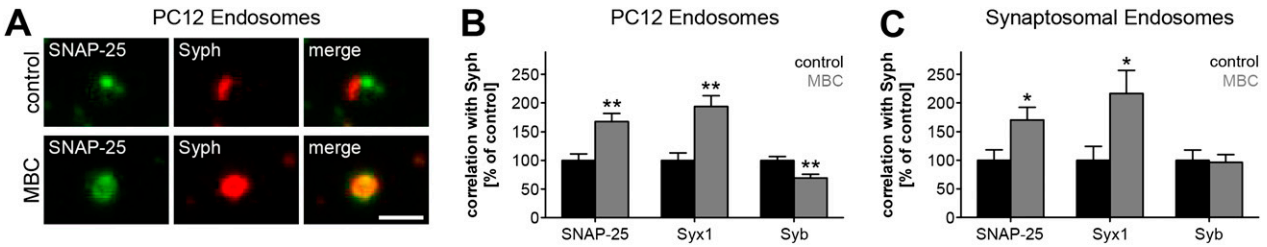

Fig. S9. Plasma membrane and synaptic vesicle markers form different domains on the endosome membrane. (*A*) PC12 bona fide endosomes immunostained for SNAP-25 (green) and synaptophysin (Syph; red) and imaged by two-color STED microscopy. (*Upper*) Control (untreated) endosomes. (*Lower*) Endosomes incubated with methyl-β-cyclodextrin (MBC) for 30 min. (Scale bar: 500 nm.) Quantification of the correlation between synaptophysin (Syph) and SNAP-25/syntaxin 1 (Syx1)/synaptobrevin (Syb), respectively, in PC12 endosomes (*B*) and synaptosomal endosomes (*C*). The Pearson's correlation coefficient was calculated for 19–176 endosomes (typically ~120 for PC12 endosomes and ~40 for synaptosomal endosomes); values are expressed as a percentage of control (black). Asterisks indicate significant changes (*$P < 0.05$; **$P < 0.01$).

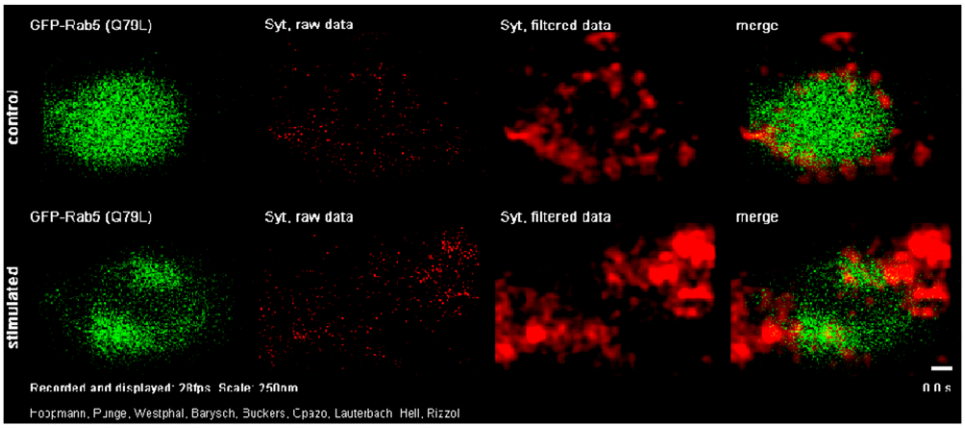

Movie S1. Live STED imaging of preparations expressing GFP-Rab5 (Q79L; green). To label synaptic vesicles, the preparations were incubated with Atto647N-coupled antibodies directed against synaptotagmin (Syt; red) for 5 min on ice before antibody wash-off (3). Images were obtained at 28 frames per second (28 Hz). The movies are presented in real-time, either at rest (*Upper*) or during 20-Hz stimulation (*Lower*). To increase the signal-to-noise ratio, the Syt raw data were filtered as described (3). Details on the imaging setup are presented in *SI Materials and Methods*. Note the slightly higher overlap between the moving vesicles and the endosomal marker in the stimulated preparation, although the vesicles are still largely avoiding the endosome.

Movie S1